

ABNORMAL ANTI-STOKES RAMAN SPECTRA OF SINGLE WALLED CARBON NANOTUBES RAISED FROM COHERENT ANTI-STOKES RAMAN SCATTERING AND OPTICAL COOLING PROCESSES

I. Baltog^{a*}, M. Baibarac^a, L. Mihut^a, S. Lefrant^b

^aNational Institute of Materials Physics, Lab. Optics and Spectroscopy,
P.O.Box MG-7, R-76900, Bucharest, Romania

^bInstitut des Matériaux de Nantes, Lab. de Physique des Matériaux et Nanostructures,
2 rue de la Houssinière, B.P.32229, 44322 Nantes, France

For the single-walled carbon nanotubes, the higher values of anti-Stokes/Stokes Raman intensity ratio (I_{as}/I_s) than the predictions of the Maxwell-Boltzmann formula indicates a CARS emission resulting from a wave mixing process between the incident laser light (ω_l) and Stokes Raman light (ω_s) generated by a SERS mechanism. The weaker value of (I_{as}/I_s) observed at resonant excitation of semiconducting nanotubes in the E_{22}^S van Hove state, relates a quantum cooling process occurred during the relaxation of the E_{22}^S excited state in two steps - by phonon emission from E_{22}^S to E_{11}^S followed by a spontaneous luminescence emission at E_{11}^S .

(Received March 26, 2007; accepted March 28, 2007)

Keywords: Carbon nanotubes, Anti-Stokes Raman Scattering, CARS, Optical cooling

1. Introduction

Single-walled carbon nanotubes (SWNTs) are as a rolled up graphene sheets into a seamless cylinders, with both ends capped with hemispheres made of hexagonal and pentagonal carbon rings [1,2]. Theoretical calculations have predicted that the electronic properties of SWNTs depend on the tube diameter d and on the helicity of the hexagonal carbon ring alignment on the nanotube surface, defined by the chiral angle θ . These calculations for the one-dimensional (1D) electronic structure of SWNTs show that about 1/3 of the nanotubes are metallic and 2/3 are semiconducting [1,2]. Both the tube diameter d and the chiral angle θ depend on the n and m integers, which denote the number of unit vectors a_1 and a_2 in the hexagonal lattice of graphite:

$$\begin{aligned} d(n,m) &= 3^{1/2} a_{C-C} (m^2 + mn + n^2)^{1/2} / \pi ; \\ \theta &= \tan^{-1} [3^{1/2} m / (m+2n)] \end{aligned} \quad (1)$$

$a_{C-C} = 1.42 \text{ \AA}$ is the nearest-neighbor C-C distance. Single-walled carbon nanotubes are metallic if $n-m = 3k$, $k = 1, 2, 3, \dots$, and semiconducting otherwise. A slight variation in these parameters causes a shift from a metallic to a semiconducting state. Whatever the synthesis method, microscopic studies have revealed that nanotubes are packed together in bundles of 20 to 100 individual tubes (1/3 metallic and 2/3 semiconducting) aligned in a two-dimensional crystal packing arrangement over essentially their entire lengths. [1,2]. The 1D electronic density of states show sharp singularities.

Raman spectroscopy is one of the widest used techniques for characterizing and understanding of properties of the carbon tubes. At resonance, when the photon energy of the excitation light corresponds to a transition between the van Hove singularities (E_{ii}) in the valence and conduction bands of a distinct nanotube, the intensity of RBM is much enhanced [1,2].

At resonance, when the exciting photon energy matches the energy separation between two van Hove singularities (E_{ii}), an occupied in the valence band and an empty in the conduction bands of a distinct nanotube,

the strong optical absorption gives rise to exceptionally high intensities for the resonant Raman effect. Such modifications are observed in the 150-200 cm^{-1} range, where one finds the bands associated with the radial breathing modes (RBM) whose frequency are inversely proportional to the tube diameter [3]. Bands belonging to the RBM, very sensitive to the excitation wavelength, play a crucial role in the characterization of SWNTs.

In particular, by using the equation $\Omega (\text{cm}^{-1}) = 223.75/d (\text{nm})$, the peak position (Ωcm^{-1}) of RBM, provides an efficient method to determine the diameters of the tubes [1,2]. The Raman signature of bundled tubes is a weaker band appearing as a shoulder up-shifted from the RBM line. The diameter of the bundled tubes from the RBM frequency can be estimated using several expressions, one of these being $\Omega (\text{cm}^{-1}) = 223.75(\text{nm} \cdot \text{cm}^{-1}) / d (\text{nm}) + \Delta\Omega (\text{cm}^{-1})$, where $\Delta\Omega = 14 \text{cm}^{-1}$ reflects the up-shift due to tube-tube interaction [3].

In the interval from 1100 to 1700 cm^{-1} two bands are found: a broad one in the range of 1500-1600 cm^{-1} , named "G" band, associated with the tangential stretching modes (TM), and another, referred to as the "D band" which is not intrinsically related to the nanotube structure, being also present in the Raman spectrum of graphitic materials. The D band is indicative of disorder induced in graphitic lattices or defects in nanotubes [1,2]. A distinguishing feature of the G band is an asymmetric component with a maximum at $\sim 1540 \text{cm}^{-1}$ that appears at laser excitation energies of 1.7–2.2 eV [1,2]. This band fits a Breit-Wigner-Fano (BWF) profile, indicating electron-phonon type interactions and corresponds to the resonant excitation of metallic nanotubes [4]. Investigations of confocal Raman microscopy combined with atomic-force microscopy (AFM) and transmission electron microscopy (TEM) have demonstrated that the BWF line is strongly enhanced in bundles of SWNTs due to the excitation of plasmon modes resulting from the inter-nanotube electrostatic interactions [5,6].

In Raman studies on SWNTs, much attention has been paid to an unusual anti-Stokes Raman effect distinguished by an abnormal intensity, sometimes increasing with the vibrational wave number, large differences in line profiles in Stokes and anti-Stokes sides and some discrepancies between the Stokes and anti-Stokes frequencies [7-18 28-39].

Normally, in conditions of thermal equilibrium, the whole structure of the Stokes and anti-Stokes Raman spectra has to be described by the Maxwell-Boltzmann law:

$$\frac{I_{\text{anti-Stokes}}}{I_{\text{Stokes}}} = \left(\frac{\omega_0 - \Omega}{\omega_0 + \Omega} \right)^4 \exp\left(\frac{hc\Omega}{kT} \right)^{-1} \quad (2)$$

where ω_0 is the exciting laser frequency, Ω the wave number of Raman line (cm^{-1}) c the light velocity, h the Planck constant and k the Boltzmann constant.

High values of the anti-Stokes/Stokes intensity ratio (I_{as}/I_s) and different line shapes of the G band are the most distinguishing features in the anti-Stokes Raman spectra of SWNTs [8,9,14,15 29,30,33,35]. The asymmetry of the Stokes and anti-Stokes spectra was generally interpreted as resulting from a double resonant Raman scattering effect produced by the excitation of different (n,m) nanotubes with the incident and Stokes scattered photons [8-10 29-31].

Nevertheless, the abnormal anti-Stokes emission has not been uniquely related with the SWNTs, in specific experimental conditions when the energy of excitation coincides with the energy of electronic transitions, it can be observed in very different materials. This is due to the fact that at resonance the third order dielectric susceptibility differs from zero, $\chi^{(3)} \neq 0$, which is basically a requirement necessary in the generation of nonlinear optical processes [19,20]

Recently, an abnormal anti-Stokes emission was accurately identified as having the characteristics of Coherent anti-Stokes Raman Scattering (CARS) [19-23]. CARS is a four-wave mixing process in which the anti-Stokes light (ω_{as}) results from the parametric coupling of the incident laser light (ω_l), the Stokes light (ω_s ; $\omega_s < \omega_l$) and a probe light (ω_p). If $\omega_l = \omega_p$ the CARS experiments appear as a degenerate four-wave mixing process that reduces to an energy transfer between the two pump waves, ω_l and ω_s .

As a general rule, the two exciting wavelengths ω_l and ω_s , are supplied by two independent lasers or are generated by parametric frequency conversion. Both alternatives make the experimental setup very complex and cumbersome. Furthermore supplementary adjustment must be carried out to assure the implementation of phase matching geometries.

New, anti-Stokes Raman spectra having the characteristics of a CARS emission were observed on different materials using a simple experimental set up under conditions of tight focusing of a single laser excitation beam [20,21]. The second pump wave, ω_s , was achieved by: i) the Surface Enhanced Raman Scattering (SERS) technique that supplied a ω_s pump light discretely distributed over all Raman transitions and situated in a broad spectral range [20] and ii) the use of only one laser light with a wide emission band, which passed through a dispersion system - diffraction grating - simultaneously supplying the two pump waves, ω_l and

ω_s . In the former case, the SERS mechanism operating over a wide spectral range furnishes ω_s for all Raman lines while in the latter case, ω_s is determined by the spectral width of the exciting light, so that the CARS effect is limited to low-wavenumber vibrational modes situated in the range of 50-400 cm^{-1} [21].

Using the micro-Surface Enhanced Raman Scattering (SERS) technique and the anti-Stokes/Stokes intensity ratio (I_{as}/I_s) as controlling parameter we demonstrate the existence of two type of anomalies in the anti-Stokes spectra of SWNT that are featured by a bigger and a smaller value of (I_{as}/I_s) ratio as resulting from the Maxwell-Boltzmann formula. In the former case operates a wave mixing process (CARS) between the incident laser light (ω_l) and Stokes Raman light (ω_s) generated by a SERS mechanism. In the latter case, the smaller value of (I_{as}/I_s) observed only for the Raman bands associated with RBM of isolated nanotubes, indicates a cooling process appearing in the semiconducting nanotubes when are resonantly excited. Generally, under resonant excitation other radiative processes are observed simultaneously with the Raman scattering. Redistribution scattering, hot luminescence, relaxed fluorescence are a few of the processes that may occur when the system can exchange energy with its environment [24]. In these terms the smaller value of (I_{as}/I_s) reveals a depopulation of the upper vibration levels of the electronic excited state by other mechanisms than conventional Raman light scattering. The most frequently is the luminescence path.

2. Experimental

SERS spectra excited with different laser power at 676.4 nm and 1064 nm were recorded in air, in backscattering geometry, using a Jobin Yvon T64000 Raman-spectrophotometer and a Bruker FT Raman S/100 spectrophotometer, respectively. Both spectrometers were fitted with a microprobe allowing the laser light to be focused to a dot on the sample with micrometer accuracy. A microscope objective of 0.95 and 0.55 numerical aperture was used. The Stokes and anti-Stokes pair spectra were recorded under the same conditions. The experiments were performed on SWNTs films of 30-150 nm thick deposited on a SERS active support. SWNTs films were obtained by evaporating a solvent (toluene) from a uniformly distributed emulsion of nanotubes on rough Au substrates. Gold SERS active substrates, with a mean roughness of about 150 nm, were prepared by vacuum evaporation.

In this work we used single-walled carbon nanotubes coming from ALDRICH and the “Groupe de Dynamique des Phases Condensées” of the University of Montpellier II.

3. Results and discussion

3.1. Abnormal anti-Stokes Raman spectra of CARS origin.

CARS is a four-wave mixing process in which the anti-Stokes light (ω_{as}) results from the parametric coupling of the incident laser light (ω_l), the Stokes light (ω_s ; $\omega_s < \omega_l$) and a probe light (ω_p). If $\omega_l = \omega_p$ the CARS experiments appear as a degenerate four-wave mixing process that reduces to an energy transfer between the two pump waves, ω_l and ω_s . In the plane-wave approximation and for a non-absorbing medium, the CARS intensity depends non-linearly on the incident pump intensity I_l :

$$I_{CARS} \propto N_A \omega_{as}^2 d^2 |\chi^{(3)}|^2 I_l^2 \text{sinc}^2(\Delta k d/2) \quad (3)$$

where $\chi^{(3)}$ is the third order nonlinear dielectric susceptibility, d is the sample slab thickness, $\text{sinc}(x)$ means $\sin(x)/x$ and N_A is the numerical aperture of the collecting lens. The coherent nature of the CARS process is reflected by the fulfilling of the phase-matching condition $|\Delta k| d \ll \pi$ where $\Delta k = k_{as} - (2k_p - k_s)$ and k_{as} , k_s and k_p are the wave vectors of the anti-Stokes, Stokes and pump light, respectively [25]. For condensed media, if the beams cross at an angle θ the small dispersion of refractive index makes $\Delta k \approx 0$ over small paths. For tightly focused beams, the requirement of phase matching relaxes, being no longer sensitive to the Raman shift and so a CARS spectrum can be observed at an angle θ_{as} larger than the Stokes angle θ_s [26,27].

Earlier studies on conducting polymers and carbon nanotubes deposited on Au or Ag substrates with an average roughness of ca. 50 nm, have shown significant variations of the SERS spectra as a function of sample film thickness [28,29]. The changes observed in Raman spectra were related to the different weights of the two basic mechanisms involved in SERS generation: i) electromagnetic, resulting from the resonant excitation of the surface plasmons and ii) chemical, mainly due to charge transfer processes between the metallic substrate and adsorbed molecules. Because the surface chemical reactions involve only few molecular layers and the penetration depth of the surface electromagnetic evanescent wave (SEEW) associated with the surface plasmons (SPs) is much larger, (≈ 12 nm metal and ≈ 95 nm in air), the selection of the film thickness is an important

parameter in SERS studies. As was showed previously an enhancement of the Raman signal through SPs can still be observed on films with a thickness up to 150 nm [28,29].

Hereinafter, the challenge is to demonstrate that at resonant laser excitation when the excitation light coincides with an electronically allowed transition ($\chi^{(3)} \neq 0$) the intensity of the anti-Stokes emission is enhanced according to eq. (3).

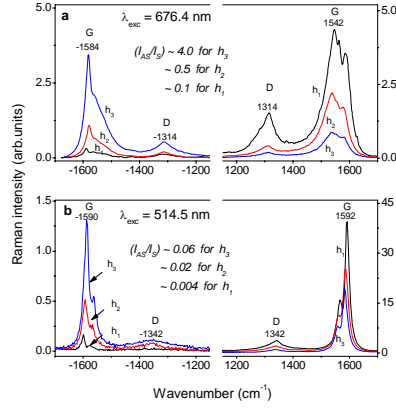


Fig.1 . Stokes and anti-Stokes SERS spectra on SWNTs films of different thicknesses ($h_1 < h_2 < h_3$ i.e, about 30, 60 and 120 nm) recorded through a microscope objective of 0.55 numerical aperture under excitation wavelengths of 676.4 , 514.5 and 1064 nm. The I_{as}/I_s ratio was estimated for the G band . Au was used as metallic SERS support.

In this frame the Fig.1 is fully relevant to demonstrate a quadratic dependence of the anti-Stokes spectra intensity on the SWNTs film thickness. The abnormal anti-Stokes Raman effect was measured by the ratio I_{as}/I_s , at $\lambda_{exc} = 676.4$ and 514.5 nm for the G band. We found values of 0.5 and 0.02 which are much bigger than $2 \cdot 10^{-5}$ that results by calculation using the eq.2. The asymmetric G band profile appearing at 676.4 nm exciting laser light indicates the strong resonant excitation of metallic nanotubes also noted by a higher value of the ratio I_{as}/I_s . Figure 1 discloses a subtle variation of the Raman intensities against the film thickness : the highest intensity is observed for the thinnest films in the Stokes side while in the anti-Stokes side for the thickest film.

This particular dependence on the film thickness is a powerful argument that in the Stokes and anti-Stokes branches operates efficiently two enhancement processes, SERS and CARS respectively. Besides, the existence of degenerate CARS process requires intrinsically two exciting lights, ω_l of the pump laser and ω_s furnished by a SERS process. The reasoning is experimentally confirmed in Fig.2 obtained for SWNTs film deposited on a porous silicon support, unable in the producing of a SERS enhancement.

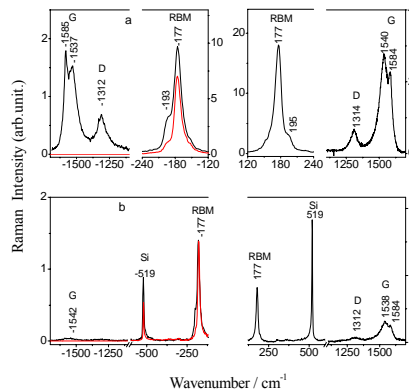


Fig.2 Stokes and anti-Stokes Raman spectra $\lambda_{exc} = 676.4$ nm on SWNTs films of ca. 60 nm thickness deposited on an active and non-active SERS support i.e, Au with ca.100 nm mean roughness (a) and porous silicon (b), respectively. The red curves illustrate the anti-Stokes Raman spectra calculated with the Maxwell-Boltzman formula applied to the measured Stokes spectra. The band at 519 cm^{-1} is the Raman signature of silicon.

Figure 2 shows that the measured anti-Stokes spectrum practically coincides with that calculated applying the formula (2) to the Stokes spectrum.

Another convincing argument for a presumed CARS emission results from exploring the variation of intensity of the anti-Stokes lines with the exciting laser power. Experimental data presented in Fig.3 display the variation as a function of laser intensity of the Raman bands at 1595 cm^{-1} (G band) in the Stokes (open symbols) and anti-Stokes (full symbols) branches. Data were obtained under varying laser intensities prior to focusing on the sample, between 25 – 150 mW (676.4 nm) and 25 – 300 mW (514.5 nm). Notice that no permanent thermal transformation of SWNTs was observed during blank experiments under identical irradiation conditions.

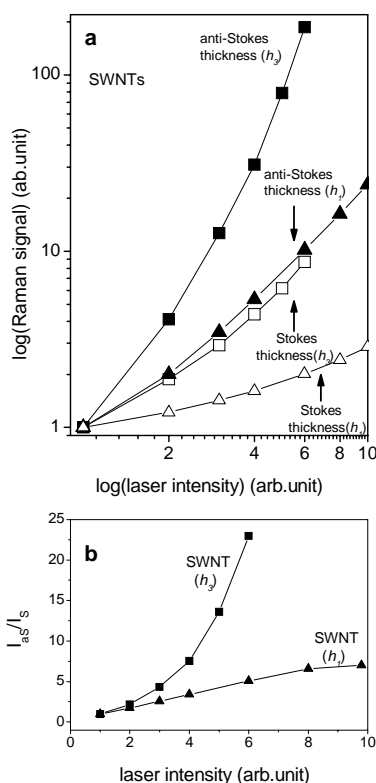


Fig.3 Anti-Stokes (full symbols) and Stokes (open symbols) Raman intensity plotted as function of laser intensity ($\lambda_{exc} = 676.4\text{ nm}$). The spectra were recorded on films of SWNTs deposited on rough Au substrate. h_1 and h_3 , notice spectra recorded on films of different thicknesses i.e. $h_1 < h_3$. The quadratic dependence of the I_{as}/I_s on incident laser intensity (Fig.b) argues a CARS type emission.

Figure 3a shows an anti-Stokes signal that increases non-linearly with the intensity of the excitation radiation. At first sight, this is not surprising - such a non-linear variation of the anti-Stokes Raman lines on the incident light power was reported for crystal violet and rhodamine 6G adsorbed on colloidal silver. It was explained as resulting from an over-population of the first excited vibration state by a spontaneous SERS effect [30]. However, Fig.3a discloses something new; the slopes of the fitted lines in a log-log plot of the dependence of anti-Stokes and Stokes emission on laser incident intensity also depend on the film thickness. Measurements performed in the spectra series of h_1 , h_2 , h_3 always reveal that the anti-Stokes component is characterized by a more abrupt slope in comparison with the Stokes emission, their values being ≈ 2 and ≈ 1 in the spectrum h_1 and >2 and >1 in the spectrum h_3 , respectively. These different slopes are not surprising if one supposes that the anti-Stokes Raman emission results from a CARS-like process in which the incident laser light mixes with the Stokes Raman scattered light generated in the sample. Together, these two contributions result in the appearance of a more complicated dependence on the incident light power. In this case, according to eq.(3), the CARS-like

emission must reveal a double dependence on the components (ω_i) and (ω_s), the latter increasing also with the incident laser light intensity.

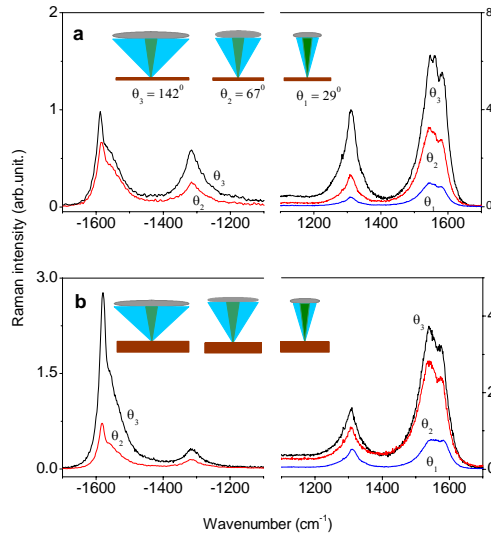


Fig.4 Stokes and anti-Stokes Raman spectra of SWNTs recorded through three microscope objectives of numerical aperture 0.95 (black), 0.55 (red) and 0.25 (blue). One used films of different thicknesses, thin (Fig.a) and thick (Fig.b). On each figure is illustrate the collecting geometry of the anti-Stokes signal.

Therefore, in Fig.3b, a I_a/I_s plot as a function of the incident power is a stronger indication of a quadratic dependence. Similar to the results shown in Fig.1, where the CARS emission appears to be more related to the thicker samples, Fig. 3 shows that the quadratic variation of the anti-Stokes Raman line intensity with the incident laser intensity is observed mainly in the spectrum h_3 , i.e. on the thicker film. Finally, these data reveal that the anti-Stokes emission originates from two different processes, a SERS one in thin films of few nanometers and a CARS one in thick films in the tens of nanometers range.

In the parametric coupling of incident laser light (ω_i) and Stokes light (ω_s), the latter is generated by a SERS mechanism in molecules situated in the proximity of the tip end of the roughness. This light, emitted in all directions, mixes with the incident laser light elsewhere in the focusing volume so that a plausible phase-matching geometry might be a planar box-wave shaped configuration or a non-planar scheme [31,32] that result in a spatial separation of the anti-Stokes Raman signal from the input laser beam. In accordance with eq. (3) such a property will be noticed by a dependence of the CARS intensity on the numerical aperture of the microscope objective used for detection. Such a dependence is quite well illustrated in Fig.4. Maintaining the same location on a SWNTs film and using microscope objectives of different numerical apertures, 0.95, 0.55 and 0.25, we obtained the spectra displayed in Fig.4. Figures 4a and 4b show spectra recorded on films of different thicknesses, thin (h_1) and thick (h_3), respectively. In the Stokes side, where the spontaneous Raman process is dominant, the intensity of Raman measured emission over the full 2π radians of a hemisphere, depends on the collection efficiency of the scattered photons so that it increases monotonically with NA . In the anti-Stokes branch, the detection of the Raman signal was possible only with a microscope objective of high NA , 0.95 and 0.55. Fig.4b discloses also a double dependence of the anti-Stokes Raman intensity on film thickness and numerical aperture. The former is related to the fact that the generation of a CARS signal needs fulfillment of the phase-matching condition and that in a box-wave shaped geometry a greater interaction volume is needed. The latter dependence is related to the CARS emission which no longer emerges uniformly from the sample, in a hemisphere of 2π radians, being concentrated in a $60-80^\circ$ angular gateway.

The same dependence of the anti-Stokes Raman intensity on the numerical aperture of the microscope objective used for the collecting the scattered light is observed on double walled carbon-nanotubes (DWNTs) at resonant excitation Fig.5.

Finally, another argument for a CARS process concerns the value of the polarization ratio in the anti-Stokes side that is always greater in comparison with that measured for a spontaneous Stokes Raman emission. This is due to the different polarization properties of the electronic and resonant portion of the $\chi^{(3)}$ which induces

in the CARS emission a different polarization ratio in comparison with the conventional spontaneous Stokes Raman scattering [33,34].

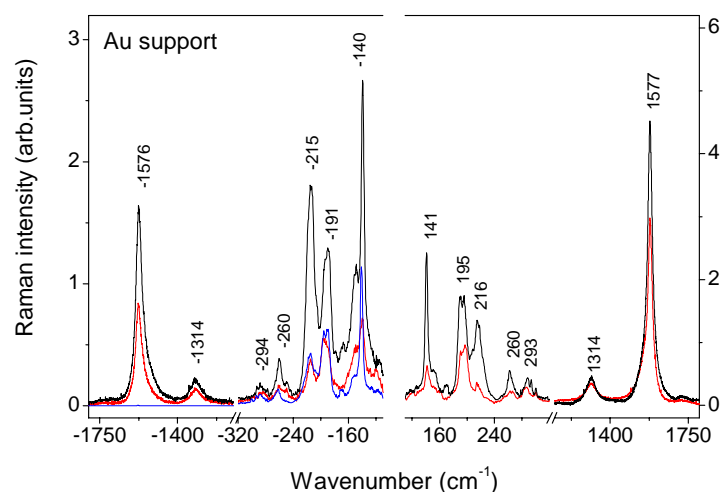


Fig. 5. Stokes and anti-Stokes Raman spectra of DWNTs recorded through two microscope objectives of numerical aperture 0.95 (black), 0.55 (red). The blue curve illustrates the anti-Stokes Raman spectra calculated with the Maxwell-Boltzmann formula applied to the measured Stokes spectrum

3.2. Abnormal anti-Stokes Raman related on an optical cooling process

It is well-known that the carbon nanotubes present a temperature-dependent effect identified in the Raman spectra by a downshift of all Raman modes. The change of phonon frequencies with temperature is a suitable technique to investigate the electronic structure and properties of carbon nanotubes. Such studies can be achieved either by increasing the temperature of the sample [35-41] or increasing the excitation laser power focused on the sample [40,41]. One must be aware that increasing the laser intensity, besides the thermal effects that can be produced, results in optical processes that, as a general rule, also occur under high density of optical excitation. The RBM, directly related to the tube diameter, is sensitive to the thermal expansion of the carbon-carbon bond so that a small down-shift of its peak is frequently observed.

Figure 6 reveals a particular aspect of the Stokes and anti-Stokes spectra of semiconducting SWNTs excited resonantly by the transition with laser light of 1064 nm of different intensities. The behavior of the two Raman bands associated with the radial vibration modes of isolated SWNTs, ($\sim 160 \text{ cm}^{-1}$) and bundled tubes ($\sim 176 \text{ cm}^{-1}$), labeled as I_{single} and I_{bundle} , respectively is discussed in relation to the wide emission band ($\sim 3100 \text{ cm}^{-1}$) that superposes the second order Raman modes within $2500\text{-}3500 \text{ cm}^{-1}$.

In conditions of thermal equilibrium, the ($I_{\text{as}}/I_{\text{s}}$) ratio reflects the temperature dependence of the relative phonon populations. It must vary in the same way for both bands, I_{single} and I_{bundle} with the increase of the sample temperature created either by directly warming the sample or indirectly increasing the exciting laser intensity focused on the sample. In Fig.6a, the temperature increasing effect at $\lambda_{\text{exc}} = 1064 \text{ nm}$ with the power varying between 25 and 250 mW is noted by a down shift estimated at $\sim 0.994\Omega$, for wall Raman lines. This means about 2 cm^{-1} for the RBM and 10 cm^{-1} for the G band; this is in good accord with other reported results [35-41]. Fig.6a shows that on the anti-Stokes side I_{bundle} and I_{single} vary differently, the former becomes more intense and increases faster than the former. Specifically we point out that I_{single} is weaker than the values predicted by the Maxwell-Boltzmann formula. Fig.6b summarizes the variations of I_{single} and I_{bundle} in the Stokes side, and the wide complex and intense band formed at cca. 3100 cm^{-1} . Clearly, the increasing rates of these three bands with the laser exciting power are different; approximately linear for I_{single} and I_{bundle} though the latter is twice as fast and the third follows an exponential term.

Figures 7a and 7b are more illustrative. They show the Stokes and anti-Stokes SERS spectra of SWNTs recorded through a microscope objective of x50 numerical aperture at two laser exciting powers ($\lambda_{\text{exc}} = 1064 \text{ nm}$; 25 and 250 mW). The laser light was focused on the sample onto a spot area of about $1 \mu^2$. The red curves

represent the anti-Stokes spectra calculated by the Maxwell-Boltzmann formula applied to the Stokes spectrum and the dotted curves show the two radial components, I_{single} and I_{bundle} , of the SWNT of about 1.4 nm diameter. At semiconducting resonance ($\lambda_{exc} = 1064$ nm) when the intensity of the exciting light varies reversibly in the range of 25-250 mW, the intensities I_{bundle} and I_{single} on the anti-Stokes side are quite the opposite of those which should be established in a state of thermal equilibrium, I_{bundle} is higher while I_{single} is weaker. This reversibility is an argument that no permanent thermal modifications of SWNTs occurred.

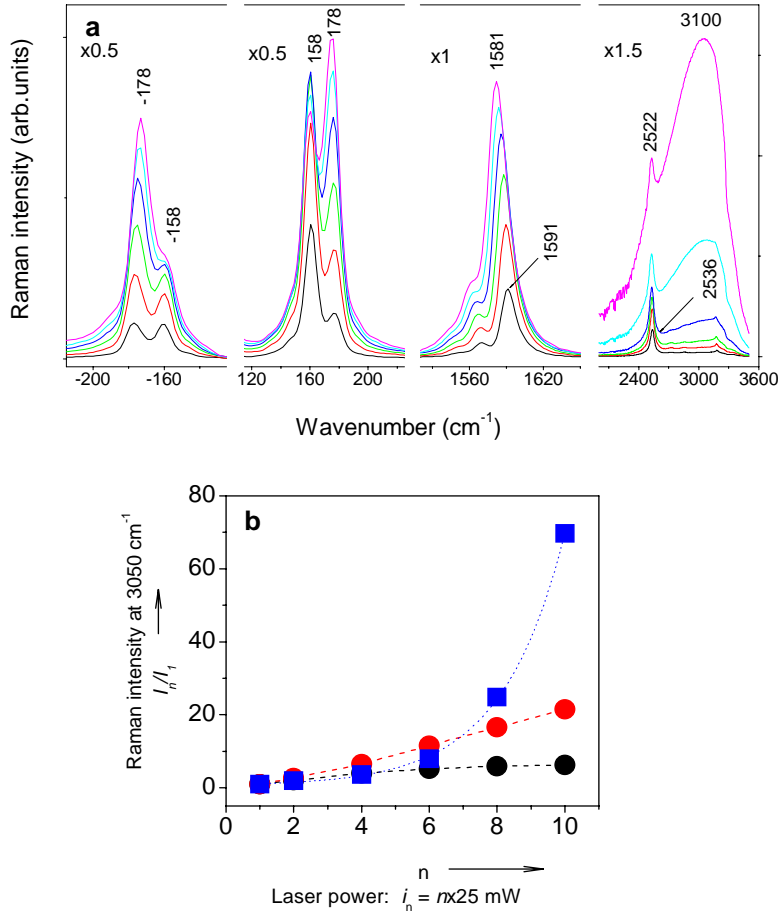


Fig.6 (a) Micro-SERS spectra of SWNTs at $\lambda_{exc} = 1064$ nm under different laser excitation power (from bottom to top: 25, 50, 100, 150, 200 and 250 mW) focused on the sample into spot area of about $1\mu m^2$. All spectra were recorded through a microscope objective of x50 numerical aperture. (b) The growth in the Stokes side of the radial bands I_{single} (black circle) and I_{bundle} (red circle) and the wide band (~ 3100 cm^{-1}) (blue square) with the laser exciting power.

Figure 7c is explicit in presenting the different variations as functions of the laser excitation power of the Raman bands I_{bundle} and I_{single} in the Stokes (full black symbols) and anti-Stokes (open black symbols) side. The open red symbols show the calculated anti-Stokes replica applying the Maxwell-Boltzmann formula to the Stokes spectra. For I_{bundle} one observes that $(I_{as}/I_s) \cong 1$ over the whole range of variation of the exciting laser power. Such a value, higher than 0.86, the limiting value towards which this ratio tends ($T \rightarrow \infty$) if the Raman process occurs in conditions of thermal equilibrium, is explicable only by supposing that on the anti-Stokes side another supplementary light scattering process operates. The abnormal anti-Stokes intensity of I_{bundle} can be well explained in the terms of CARS emission generated in the nanometric thin films by mixing of the exciting wavelengths, ω_l , with the Raman Stokes light, $\omega_s(bundle)$.

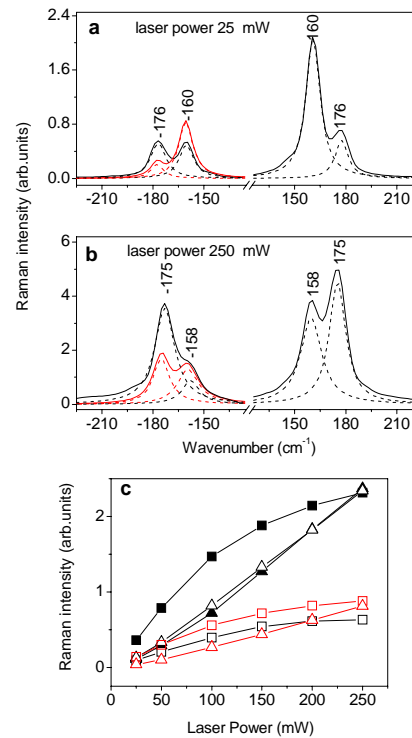


Fig.7. Stokes and anti-Stokes micro-SERS spectra (black curves) of SWNTs under different power excitation (25 mW -a ; 250 mW-b) focused into spot area of about $1\mu\text{m}^2$ ($\lambda_{\text{exc}} = 1064\text{ nm}$).All spectra were recorded through a microscope objective of x50 numerical aperture. In The red curves represent the anti-Stokes spectra calculated applying the Maxwell-Boltzmann formula to the Stokes spectra. Dotted curves figure the two components of RBM, associated to the individual (160 cm^{-1}) and bundled tubes (177 cm^{-1}). In c is presented the variation of the intensity of bands (160 cm^{-1} (square) and 177 cm^{-1} (triangle) in the Stokes (full symbol) and anti-Stokes (open symbol) branches versus laser exciting intensity. The open red symbols figure the anti-Stokes signals calculated with the Maxwell-Boltzmann formula.

As arguments one can invoke the approximately square relationship between the CARS signal intensity and film thickness and the exciting laser intensity, a dependence of the CARS intensity on the numerical aperture (NA) of the microscope objective used for detection of anti-Stokes emission and a greater polarization ratio on the anti-Stokes side compared with that measured on the Stokes side [20].

Interesting is the different behavior on the anti-Stokes side observed for the band at 160 cm^{-1} , associated with the isolated nanotubes (I_{single}). In the SWNTs of $\sim 1.4\text{ nm}$ diameter, the excitation (1064 nm) activating an electronic transition from ground state to the E_{22}^S level of semiconducting tubes, imposes features of resonance on the Raman process [1,2]. Generally, under resonant excitation other radiative processes are observed simultaneously with the Raman scattering. In such cases the anti-Stokes Raman intensity deviates from that established by the Maxwell-Boltzmann formula, it is weaker appearing as result of a vibrational cooling effect.

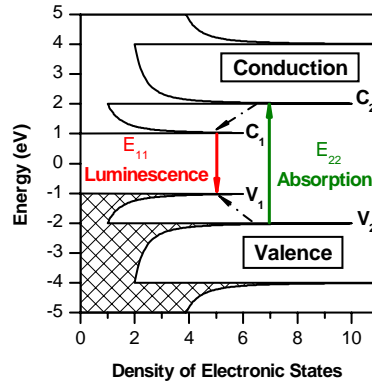


Fig. 8. Scheme of the luminescence emission from the E_{11}^S state of semiconducting SWNT populated by the phonon relaxation of the optical E_{22}^S excited level.

Returning to the SWNTs, the transition to the E_{22}^S level creates an (eh_{22}) exciton. Satisfying the requirements of energy-momentum conservation the relaxation from E_{22}^S to the ground state may occur by a Raman process or either Raman and luminescence processes. Indeed, it has been demonstrated that the relaxation of E_{22}^S excited semiconducting nanotubes occurs in two steps - by phonon emission from E_{22}^S to E_{11}^S followed by a spontaneous luminescence emission at E_{11}^S [42-45]. A scheme of the process illustrated in Fig.8 reveals that the phonon relaxation resemble with a carriers cooling process of the hot holes and electrons. The two emitted phonons are gotten in the environment, in the bundle of nanotubes, which explains why in the Fig.6b was found for the I_{bundle} an increasing rates with the laser exciting power twice as fast then I_{single} .

In this context the question arises of whether the complex emission band observed at cca. 3100 cm^{-1} (Fig.6a) can be considered as a luminescence band intrinsically related to the semiconducting nanotubes resonantly excited with 1064 nm or whether it must be associated with a compound resulting from the thermal transformation of the nanotubes. Analysis of experimental data makes the latter explanation hardly acceptable. An eventual thermal transformation of nanotubes ended by a new compound developing gradually with the increased the laser exciting intensity is expected to be an irreversible process, such a compound must be observed constantly after performing the first cycle of measurements. This expectation is not fulfilled by the experimental facts. The Raman spectra obtained with exciting light of 1064 nm, which contains the broad emission band peaking around 3100 cm^{-1} , change reversibly on increasing or decreasing the laser excitation intensity.

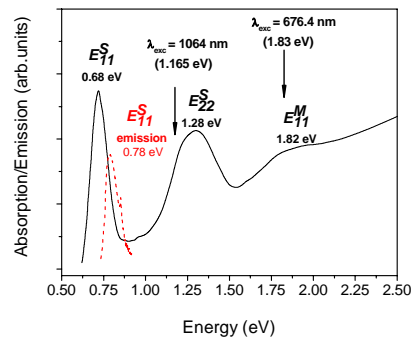


Fig. 9. Absorption (full line) and emission (dashed red line) spectra of SWNTs of 1.4 nm diameter. The emission (dashed red line) spectra under excitation light of $\lambda_{exc} = 1064\text{ nm}$ has been recorded simultaneously with the Raman spectrum.

Moreover, such a emission band, associated with a luminescence process, and varying reversibly in the intensity range of 25-250 mW of the $\lambda_{\text{exc}} = 1064$ nm is constantly observed in various types of nanotubes, single-walled, double-walled or multi-walled. The unique difference is that the threshold beyond which one can detect a nonlinear growth of the intensity appears at different intensities of the laser exciting light. The absence of this luminescence band in the Raman spectrum at $\lambda_{\text{exc}} = 676.4$ nm, which activates the E_{11}^M interband electronic transitions, encourages us to suppose that it is strongly associated with the semiconducting nanotubes. In this context another question immediately arises. Using $\lambda_{\text{exc}} = 1064$ nm, why does the wide luminescence band around 3100 cm^{-1} become observable predominantly at higher intensities of exciting light when sample heating takes place. The answer must given taking into consideration the temperature sensitivity of the intrinsic photoluminescence of a semiconductor submitted to a band to band excitation. In this sense a special behavior must be borne in mind. In general, a semiconductor under laser excitation of energy accommodated to its band gap edge, presents an intrinsic edge luminescence that shifts towards lower energies with the increase of the laser intensity. Two facts compete to this result one related of increasing of the excitons density which recombining radiatively generate a more intense emission and other of thermal nature appearing under focused exciting light that produces a narrowing of the band gap edge. Another explanation invokes the internal absorption caused by an exponential absorption tail at the band edge. A particular situation is met when the energy of excitation is a little lower than the band gap edge and the luminescence excitation does not occur. Under focused excitation, due to the local heating of the sample, a thermal narrowing of the bad gap takes place resulting in better accommodation with the energy of excitation. In this way the condition of resonant excitation is achieved that is able to explain the appearance and the enhancement of an intrinsic edge luminescence. Such a situation apparently occurs in our case. In contrast, when the energy of the excitation coincides with the band gap edge a disappearance of the intrinsic luminescence can be observed as the sample cools. . By cooling the sample, its band gap increases so that the energy of excitation light is no longer sufficient for the band gap edge transition. A significant detail supporting the above comment is that at $\lambda_{\text{exc}} = 676.4$ nm when the E_{11}^M interband electronic transitions of metallic nanotubes is activated, the Raman spectrum lacks any luminescence despite the fact that such exciting light, being of higher energy, should be more efficient in the excitation of luminescence.

Fig.9 shows the absorption spectrum of the SWNTs studied in this paper. Three absorption bands at 0.68, 1.28 and 1.82 eV which are associated with the transitions from the ground state in the E_{11}^S and E_{22}^S states of semiconducting tubes and the E_{11}^M state of metallic tubes, respectively, can be identified.

Returning to Fig.6a we consider the wide band located around 3100 cm^{-1} in the Raman spectrum of SWNTs at $\lambda_{\text{exc}} = 1064$ nm (1.165 eV) as being a luminescence band due to the relaxation of the E_{22}^S excited state via the E_{11}^S level . Actually, its real peak position in the energy scale is at 0.78eV. In Figure 9, this emission band (dotted curve), overlaid with the absorption spectrum of the studied SWNTs, accommodates very closely with the low energy side of the E_{11}^S absorption band. Unfortunately, technical restrictions imposed by the spectrophotometer (upper measuring limit 3500 c^{-1}), cause truncation of this band on its high energy side. In spite of this inconvenience and in the base of other reported data presenting the coincidence between E_{11}^S absorption and luminescence band of SWNTs [42,46], the matching of position and profile with the high side of E_{11}^S absorption band argues that the emission band at 3100 cm^{-1} observed in the Raman spectrum at $\lambda_{\text{exc}} = 1064$ nm of SWNTs can be attributed the radiative de-excitation of the E_{11}^S level.

Taking the above observations into account we are tempted to conclude that the cooling effect noted in the Raman spectrum by lowering of $(I_{\text{as}}/I_{\text{s}})$ ratio adjacent to the Raman band associated with the isolated nanotubes is mainly related to the semiconducting nanotubes. This suggests a phonon emission step in the de-excitation of the E_{22}^S state. Indeed, the other experimental results also support this conclusion. For this it is sufficient to consider Figure 10 in which the Stokes and anti-Stokes Raman spectra at $\lambda_{\text{exc}} = 676.4$ nm, are shown. This wavelength corresponds to the resonant excitation of metallic nanotubes. [1,2]. Just as in Fig.6 the Raman band associated with the RBM has two components at 176 and 194 cm^{-1} which indicate the isolated and bundled nanotubes, respectively, (Fig.6a).

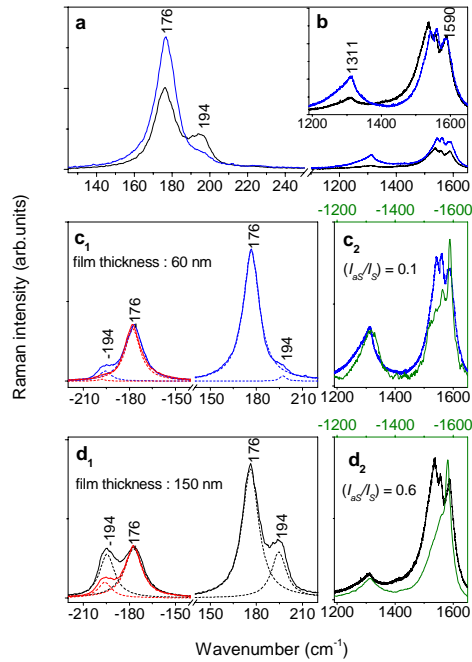


Fig.10. Stokes and anti-Stokes micro-SERS spectra of SWNTs thin films, of about 60 (black) and 150 nm (blue) thickness at laser excitation light of 200 mW ($\lambda_{exc} = 676.4$ nm) focused on spot area on the sample of about $1\mu\text{m}^2$. All spectra were recorded through a microscope objective of $\times 50$ numerical aperture. In **b** are presented into normalized scale the Raman spectra in the range of $1200\text{--}1650\text{ cm}^{-1}$ where are situated the D (1131 cm^{-1}) and G (1590 cm^{-1}) bands. The red curves represent the anti-Stokes replica calculated applying the Maxwell-Boltzmann formula to the Stokes spectra. In **c**₁ and **d**₁ the dotted curves figure the two components of RBM, one associated to the individual tubes (176 cm^{-1}) and bundled tubes (194 cm^{-1}). In **c**₂ and **d**₂ are presented the D and G bands in Stokes and anti-Stokes (green curves) side.

Their relative intensities vary with the film thickness and the band associated with the tubes in bundles becomes more prominent with increased film thickness. A distinguishing feature of the G band is an asymmetric profile appearing at laser excitation energies of $1.7\text{--}2.2\text{ eV}$ that correspond to the resonant excitation of metallic nanotubes [1,2].

Comparing Figs.6 and 10 the latter reveals important differences in the anti-Stokes side such as i) an abnormally intense anti-Stokes spectrum developed over a large spectral range, including the D and G bands, and ii) different behaviors of the components I_{bundle} and I_{single} . That is, only the former line displays an increased intensity while the latter shows an identical profile in good agreement with the predictions of the Maxwell-Boltzmann formula. According with the eq. (3) the high intensities of the D and G bands on the anti-Stokes side result from the square relationship between the intensity of anti-Stokes signal and the anti-Stokes Raman frequencies, typical for a CARS process.

In Figs. 10c₁ and 10c₂, the ratio (I_{as}/I_s) increases quadratically, i.e., from 0.1 to 0.6, with the increase in the film thickness. For the I_{bundle} approximately the same variation was found. In this context, using laser excitation of $\lambda_{exc} = 676.4\text{ nm}$, it is worth pointing out the absence of an enhanced luminescence on increasing the exciting laser intensity has now been observed at $\lambda_{exc} = 1064\text{ nm}$.

4. Conclusions

An inciting and much debated subject in the Raman studies on SWNTs is an unusual anti-Stokes Raman spectrum distinguished by an abnormal intensity, increasing with the vibrational wave number, large differences in line profiles in Stokes and anti-Stokes sides and some discrepancies between the Stokes and anti-Stokes frequencies. For interpretation has been invoked a double resonant Raman scattering effect produced by

the excitation of different (n,m) nanotubes with the incident and Stokes scattered photons. Nevertheless, the abnormal anti-Stokes emission has not been uniquely related with the SWNTs, in specific experimental conditions when the energy of excitation coincides with the energy of electronic transitions, it can be observed in very different materials. This is due to the fact that at resonance the third order dielectric susceptibility differs from zero, $\chi^{(3)} \neq 0$, which is a requirement necessary in the generation of nonlinear optical processes. In this paper, we have presented another explanation of the abnormal anti-Stokes Raman spectra that appears at resonant optical excitation.

Using the anti-Stokes/Stokes Raman intensity ratio (I_{as}/I_s) as analyzing parameter, the comparison with its value predicted of the Maxwell-Boltzmann formula reveals a higher value for the anti-Stokes Raman lines of SWNTs. We demonstrate that under a tight-focusing of the excitation light, a CARS emission resulting from a wave mixing process between the incident laser light (ω_i) and Stokes Raman light (ω_s) generated by a Surface Enhanced Raman Scattering (SERS) mechanism is produced. The CARS emission is argued by: i) a square relation between the CARS signal intensity and the film thickness; ii) a square relationship between the CARS signal intensity and the exciting laser intensity; iii) a dependence of the CARS intensity on the numerical aperture (NA) of the microscope objective used for the detection of the anti-Stokes emission; iv) a polarization ratio in the anti-Stokes side always greater in comparison with that measured for a spontaneous Stokes Raman emission.

The generality of this effect is violated of the behavior of the Raman line associated with the RBM of isolated nanotubes, for which (I_{as}/I_s) is weaker than its value ordered of the thermal equilibrium rules. This particular behavior, observed at resonant excitation of semiconducting nanotubes in the E_{22}^S van Hove state, relates a quantum cooling process occurred during the relaxation of the E_{22}^S excited state in two steps - by phonon emission from E_{22}^S to E_{11}^S followed by a spontaneous luminescence emission at E_{11}^S .

References

- [1] M.S.Dresselhaus, G.Dresselhaus, A.Jorio, A.G.Souza Filho, R.Saito, Carbon, **42**,2043,(2002) and references therein
- [2] M.S.Dresselhaus, G.Dresselhaus, R.Saito, A.Jorio, Physics Reports **409**, 47, (2005) and references therein
- [3] Bandow S, Asaka S, Saito Y, Rao A M, Grigorian L, Richter E, and Eklund PC, Phys. Rev. Lett. **80**, 3779 (1998)
- [4] M.A.Pimenta, A.Marucci, S.A.Empedocles, M.G.Bawendi,E.B.Hanlon, A.M. Rao, C.Eklund, R.E.Smalley,G.Dresselhaus, and M.S. Dresselhaus, Phys. Rev. B, **58**, R16016 (1998)
- [5] C.Jiang, K.Kempa, J.Zhao, U.Schlecht,U.Kolb, T.Basche, M.Burghard, and A. Mews Phys.Rev. B **66** 161404 (2002)
- [6] M.Paillet, Ph.Poncharal,A.Zahab, and J.-L.Sauvajol Phys. Rev. Lett. **94** 237401 (2005)
- [7] P-H. Tan, Y.M. Deng and Q.Zhao Phys. Rev. B **58**, 5435 (1998)
- [8] S.D.M.Brown,P.Corio,A.Marucci, M.S.Dresselhaus, M.A.Pimenta and K. Kneipp, Phys. Rev. **61** R5137 (2000)
- [9] K.Kneipp, H.Kneipp, P.Corio, S.D.M.Brown, K.Shafer,J.Motz,,L.T.Perelman,E.B.Hanlon, A.Marucci, G.Dresselhaus and M.S.Dresselhaus, Phys. Rev. Lett. **84**, 3470 (2000)
- [10] C.Thomsen and S.Reich, Phys.Rev.Lett.**85**, 5214 (2000)
- [11] A.K. Sood ,R.Gupta and S.A.Asher J.Appl.Phys.**90**, 4494 (2001)
- [12] A.G.Souza-Filho, A.Jorio ,J.H. Hafner,C.M.Lieber, R.Saito, M.A.Pimenta, G.Dresselhaus and M.S.Dresselhaus, Phys.Rev. B **63**, 241404 (2001)
- [13] A.Jorio, A.G.Souza-Filho,G.Dresselhaus, M.S.Dresselhaus, R.Saito ,J.H. Hafner,C.M.Lieber, F.M.Mantinaga, M.S.S.Dantas and M.A.Pimenta, Phys.Rev. B **63**, 245416 (2001)
- [14] S-L. Zhang ,X. Hu, H.Li, Z.Shi, K.T.Yue, J.Zi,Z. Gu, X.Wu, Z.Lian, Y.Zhan, F.Huang, L. Zhou,Y. Zhang and S.Ijimia, Phys. Rev. B **66**, 035413 (2002)
- [15] L.G Cancadao, M.A.Pimenta,R.Saito, A.Jorio,L.O. Ladeira, A. Grüeneis,A.G. Souza-Filho,G.Dresselhaus and M.S.Dresselhaus, Phys.Rev.B**66**, 035415 (2002)
- [16] V.Zolyomi and J.Kurti, Phys.Rev. B **66**, 073418 (2002)
- [17] P-H.Tan, L. An, L-O.Liu ,Z-X. Guo, R.Czerw, D.L.Carroll, P.M.Ajayan, N.Zhang and H-L.Guo Phys. Rev. B **66**,245410 (2002)
- [18] A.G.Souza-Filho,S.G.Chou,G.G.Samsonidze, G.Dresselhaus, M.S. Dresselhaus, L. An, J.Liu, A.K.Swan, M.S. Ünlü, B.B.Goldberg, A.Jorio,A. Grüeneis and R.Saito, Phys.Rev. B **69**, 115428 (2004)
- [19] I.Baltog, M.Baibarac, and S.Lefrant, 2005 Journal of Optics A: Pure and Applied Optics **7**, 1 (2005)

- [20] I.Baltog, M.Baibarac, and S.Lefrant, Phys Rev B, **72**, 245402 (2005)
- [21] D.Mehtani, N.Lee, R.D.Hartschuh, A.Kisliuk, D.Foster, A.P.Sokolov, J.F.Maguire, J.Raman Spectrosc. **36**, 1068 (2006)
- [22] B.Vacano, W.Wohlleben, M.Motzkus, J.Raman Spectrosc. **37**, 404 (2006)
- [23] Z.D.Schultz, M.C.Gurau, L.J.Richter, Applied Spectrosc. **60**, 1097 (2006)
- [24] Topics in Current Physics vol.11 *Raman Spectroscopy of gases and liquids*, editor A.Weber; Springer-Verlag, Berlin (Chap.6 *The Resonance Raman Effect*, by D.L.Rousseau, J.M.Fiedeman, P.F.Williams, 1979)
- [25] Y.R.Shen *The Principle of Nonlinear Optics* (New York: Wiley 1984)
- [26] M.Müller and J.M.Schins, J.Phys.Chem.B **106** 3715 (2002)
- [27] J.X.Cheng, A.Volkmer, L.Book and X.S.Xie Phys.Chem.B **106**, 8493 (2002)
- [28] M.Baibarac, L. Mihut, G.Louarn, S.Lefrant and I.Baltog, J Polymer Science Part B **38**, 2599 (2000)
- [29] S.Lefrant, I. Baltog, M.Baibarac, J.Schreiber and O.Chauvet, Phys. Rev. B **65**, 235401 (2002)
- [30] K.Kneipp, Y.Wang, H.Kneipp, I.Itzkan, R.R.Dasari and M.S.Feld, Phys.Rev.Lett. **76**, 2444 (1996)
- [31] M.Müller and J.M.Schins, J.Phys.Chem.B **106**, 3715 (2002)
- [32] J.X.Cheng, A.Volkmer, L.Book, and X.S.Xie, Phys.Chem.B **106**, 8493 (2002)
- [33] R.M.Martin and L.M.Falikov *Light Scattering in Solids I*, edited by M.Cardona, Topics in applied Physics. vol.8 (Berlin: Springer) (1983)
- [34] Y.Saito, T.Ishibashi, H.Hamaguchi, J.Raman Spectrosc. **31**, 725 (2000)
- [35] P.V.Huong, R.Cavagnat, P.M.Ajayan, O.Stephan, Phys.Rev.B **51**, 10048 (1995)
- [36] F.Huang, K.T.Yue, P.Tan, S.L.Zhang, Z.Shi, X.Zhou, Z.Gu, Appl.Phys.Lett. **84**, 4022 (1998)
- [37] N.R.Raravikar, P.Keblinski, A.M.Rao, M.S.Dresselhaus, L.S.Schadler, P.M.Ajayan Phys Rev B. **66**, 235424 (2002)
- [38] Z.Zhou, X.Dou, L.Ci, L.Song, D.Liu, Y.Gao, J.Wang, L.Liu, W.Zhou, S.Xie J.Phys.Chem.B **110**, 1206 (2006)
- [39] S.B.Cronin, Y.Yin, A.Walsh, R.B.Capaz, A.Stolyarov, P.Tangney, M.L.Cohen, S.G.Louie, a.K.Swan, M.S.Unlu, B.B.Goldberg, M.Tinkham, Phys.Rev.Lett. **96**, 127403 (2006)
- [40] Q.Zhang, D.J.Yang, S.G.Wang, S.F.Yoon, J.Ahn, Smart Mater. Struct **15**, S1-S4, (2006)
- [41] Y.Quayang and Y.Fang, Physica E **24**, 222 (2004)
- [42] S.M.Bachilo, M.S.Strano, C.Kitrell, R.H.Hauge, R.E.Smalley, R.B.Weisman, Science, **298**, 2361 (2002)
- [43] C.L.Kane, E.J.Mele, Phys.Rev.Lett. **90**, 207401 (2003)
- [44] S.Reich, C.Thomsen, J.Robertson, Phys.Rev.Lett. **95**, 077402 (2005)
- [45] Y.Oyama, R.Saito, K.Sato, J.Jiang, G.G.Samsonidze, A.Gruneis, Y.Miyauchi, S.Maruyama, A.Jorio, G.Dresselhaus, S.Dresselhaus Carbon, **44**, 873 (2006)
- [46] F.Wang, G.Dukovic, L.E.Brus, T.F.Heinz, Phys.Rev.Lett. **92**, 177401 (2004)